Analyst

Accepted Manuscript

This article can be cited before page numbers have been issued, to do this please use: M. Roman, C. Rigo, H. Castillo-Michel, D. S. Urgast, J. Feldmann, I. Munivrana, V. Vindigni, I. Mieti, F. Benetti, C. Barbante and W. R. L. Cairns, *Analyst*, 2020, DOI: 10.1039/D0AN00607F.

Spatiotemporal distribution and speciation of silver nanoparticles in the healing wound

View Article Online
DOI: 10.1039/D0AN00607F

Marco Roman[1*], Chiara Rigo[1], Hiram Castillo-Michel[2], Dagmar S. Urgast[3], Jörg Feldmann[3], Ivan Munivrana[4], Vincenzo Vindigni[4], Ivan Mičetić[5], Federico Benetti[6], Carlo Barbante[1,7], Warren R.L. Cairns[7]

[1] Ca' Foscari University of Venice, Department of Environmental Sciences, Informatics and Statistics (DAIS), Via Torino 155, 30172 Venice Mestre, Italy
[2] European Synchrotron Radiation Facility (ESRF), 71 avenue des Martyrs, 38000 Grenoble, France
[3] University of Aberdeen, Trace Element Speciation Laboratory, Aberdeen AB24 3UE, Scotland UK
[4] University Hospital of Padua, Burns Centre, Division of Plastic Surgery, Via Giustiniani 2, 35128 Padua, Italy
[5] University of Padua, Department of Biomedical Sciences, Via Ugo Bassi, 58/B35131 Padua, Italy
[6] EcamRicert Srl, European Centre for the Sustainable Impact of Nanotechnology (ECSIN), Corso Stati Uniti, 4 35127 Padua, Italy
[7] Institute for Polar Sciences (ISP-CNR), Via Torino 155, 30172 Venice Mestre, Italy

*** Correspondence:**
Marco Roman
Ca' Foscari University of Venice, Department of Environmental Sciences, Informatics and Statistics (DAIS), Via Torino 155, 30172 Venice Mestre, Italy
Phone: +0039 041 234 7731
E-mail: marco.roman@unive.it

Keywords: Silver nanoparticles (AgNPs); Wound healing; Burn; Elemental imaging; Elemental speciation; Synchrotron radiation; Laser ablation ICP-MS.

View Article Online
DOI: 10.1039/D0AN00607F

Abstract

The medical application of nanomaterials is growing fast. Amongst the most widely used, silver nanoparticles are antimicrobial agents whose key application is the care of burns and chronic wounds. Still, their absorption, distribution, metabolism and excretion behaviour *in vivo* has not yet been systematically investigated. We collected full-profile specimens of skin from four hospital patients with mid-to-deep thickness burns or equivalent skin wounds, treated with dressings containing silver nanoparticles or silver sulfadiazine. Synchrotron radiation µXRF/µXANES and laser ablation-ICP-MS were used to provide the first semi-quantitative/high resolution direct information on the spatiotemporal distribution and speciation of silver *in vivo*. The metal was rapidly released onto the wound surface, followed by a significant structure-dependent penetration into the damaged tissues. This was accompanied by sequential processes of metallic silver dissolution, chloride complexation, change to metal-thiol protein complexes, and final mobilization into deeper skin layers towards the vascular networks. Complete local clearance of silver was observed after 12 days of treatment in the case of full healing. The results provide a complete insight into the dynamics of silver in real human wounds, and a new basis for the design of innovative silver nanomaterials with optimal antibacterial efficacy and minimized risk for the patient.

View Article Online
DOI: 10.1039/D0AN00607F

List of the acronyms

Ag	silver
BSA	bovine serum albumin
DLS	dynamic light scattering
ECM	extracellular matrix
ELS	electrophoretic light scattering
ESRF	European Synchrotron Radiation Facility
GSH	glutathione
HINS	human insulin
HSA	human serum albumin
HSS	human serum substitute
HTF	human transferrin
LA-ICP-MS	laser ablation-inductively coupled plasma-mass spectrometry
LCF	linear combination fitting
MALDI-TOF-MS	matrix-assisted laser desorption time-of-flight mass spectrometry
MMPs	matrix metalloproteinases
MTs	metallothioneins
NPs	nanoparticles
PDI	polydispersity index
ROS	reactive oxygen species
SEM-EDX	scanning electron microscopy - energy dispersive X-ray spectroscopy
SR-μXANES	synchrotron radiation X-ray absorption near edge structure
SR-μXRF	synchrotron radiation micro x-ray fluorescence

View Article Online
DOI: 10.1039/D0AN00607F

1 Introduction

Burn injuries are a critical care problem of high concern for public health. Severe burns may be life threatening due to extensive loss of plasma, specific and systemic immunological response, bacterial infections and septicemia.[1] The management of wound bed in burns requires dedicated treatment protocols, different from all the other types of wound, whose quality is fundamental for stabilizing the patient, preventing the infection and optimizing tissue regeneration, but also for the long-term metabolic, functional and esthetical recovery.[2]

Silver (Ag) has been used since ancient times in the treatment of burns and chronic skin lesions due to its observational efficacy in promoting tissue repair. Only over the last century the specific capacity of Ag to inhibit microbial growth were elucidated and systematically exploited in clinical settings to protect the wound against infection, a critical complication which can slow down or even prevent, the spontaneous regeneration of damaged tissues.[3] The metal is now well known as an effective multispectral antibacterial, antiseptic, and anti-inflammatory agent. Its antimicrobial action unfolds through multiple pathways, resulting in limited onset of bacterial resistance and effectively preventing biofilm formation.[4–7] The bioactive species of the metal is the Ag^+ ion, which binds to the cell wall of bacteria and deactivates many enzymes vital for their metabolism. However, the ion is also prone to rapid inactivation by binding to chloride or biomolecules in the wound microenvironment.[8,9] This makes local application the only effective treatment with Ag as this ensures sustained concentrations of its ionic form on the surface layer of the wound bed. Indeed, medications containing Ag(I) species, such as Ag nitrate solutions and Ag sulfadiazine creams (widely used for the emergency treatment of burns) require multiple daily applications to remain effective.[10] Great efforts are currently underway to develop innovative materials that ensure an effective and modulated antibacterial action of Ag, with concomitant minimum dosage, preserved hydration, mediated cells transferring to the wound, and general comfort for the patient. A new generation of Ag-based dressings have been designed, consisting of biocompatible scaffolds (meshes, foams, gels or composites) impregnated with Ag as soluble salts, AgCl, microcristalline Ag sulfadiazine, or as a metallic film.[11,12] One of the most promising approaches bases on metallic Ag nanoparticles (AgNPs).[13] The nanoparticulate forms of Ag exhibit unique physico-chemical properties such as nanometric size, crystal structures and enhanced surface reactivity, which can be specifically designed for an improved stability in biological media,[10,14] enhanced affinity for cellular membranes to favour the uptake, and calibrated dissolution for delivery of the ion to intracellular targets.[6,15,16] Several new dressings with AgNPs have been developed over the last years and tested *in vitro* for their antibacterial efficacy, including functionalized nanofibers,[17] impregnated hydrogels,[18] and doped bio-nano composite foams and films.[19] An extensive review of these materials has been published recently.[20] A growing body of evidence supports the clinical effectiveness of the few dressing loaded with AgNPs that are already being employed in hospitals,[21–25] and the medical use of AgNPs is therefore expected to expand rapidly in the near future.

However, great concern remains in the scientific community regarding the safety implications of the administration of AgNPs to humans,[26] because the moderate cytotoxicity of Ag^+ towards skin

cells is also well documented,[10,27,28] and contradictory effects on wound re-epithelialisation have been reported after use of Ag-containing dressings.[21,22] It is now generally accepted that AgNPs do not exert any specific toxic action,[14,21,29] but as they carry out a modulated delivery of Ag^+, toxicity through indirect mechanisms is supposed. Particularly, endocytic uptake of AgNPs leads to direct delivery of Ag^+ ions to the intracellular environment, where they interact with thiol groups of mitochondrial membrane proteins, causing a cascade of cellular dysfunctions mediated by reactive oxygen species (ROS) generation.[28] Alteration of DNA and chromosomal breakage has been also reported, in association with AgNPs penetration into the nucleus.[28] As observed for antibacterial efficacy, these toxic effects are size- and shape-dependent because AgNPs morphology impacts their penetration ability and surface reactivity.[30]

Designing materials and defining usage protocols to achieve optimal *in vivo* efficacy with a minimum dosage and risk for the patient requires a detailed knowledge of the dynamics of Ag in the human body. This knowledge is currently incomplete.

The chemical behaviour of AgNPs in the wound can be inferred from theoretical models and from limited experiments on dissolution, administration to cell cultures and percutaneous permeation carried out *in vitro* or *ex vivo*. Most studies indicate that although absorption of the metal through intact skin may be exceedingly low,[22,23,31,32] damage to the skin barrier as happens in a wound could significantly favour penetration.[33,34] A positive correlation between blood Ag level and wound extent or severity observed in patients treated with AgNPs supports this theory.[23,24,35,36]

Still, it remains unclear whether Ag is mobilized as active pristine NPs, or as deactivated biocomplexes of the ionic form. This issue is the key for predicting the local and systemic activity of the absorbed metal. Simplified *in vitro* experiments suggest several possibilities for biochemical processes involving AgNPs *in situ*, including: oxidative dissolution,[9,27,37] surface interaction with biomolecules and exchange of free Ag^+ ions,[9,37] as well as photoreductive generation of secondary nanoparticulate species.[8,34] However, direct observations describing how these processes interact in time and space *in vivo* have not been provided so far. *In vivo* rodent burn models are limitedly reliable because their wounds heal following different mechanisms, and do not exude fluids as human lesions do.[38,39] Pigs are the best choice for preclinical evaluations,[38] but only a few data are available on the total deposition of Ag in the scar of a porcine burn model so far.[40]

This study provides the first direct observation of the spatiotemporal distribution and chemical transformations of Ag in the wounds of four real patients (A-D), who underwent clinical treatment with a commercial dressing containing AgNPs, namely Acticoat Flex3™. Full-profile biopsy samples were collected from the wound beds at different time steps from admission to complete healing. They were analysed by the high resolution elemental imaging methods of synchrotron radiation micro x-ray fluorescence (SR-μXRF) and laser ablation-inductively coupled plasma-mass spectrometry (LA-ICP-MS), and the chemical speciation of Ag was determined by synchrotron radiation X-ray absorption near edge structure (SR-μXANES) analysis. The results show how Ag nanoparticles and ions interact with bioligands while migrating within the skin wound, as a function of its structural damage and healing progression.

View Article Online
DOI: 10.1039/D0AN00607F

2 Experimental

An extended version of this methods section can be found in Supplementary Information, inclusive of additional details on the experimental conditions and approaches, and a comparison of the analytical performances of SR-μXRF and LA-ICP-MS.

2.1 Characterization of the dressing and release of Ag *in vitro*

Extensive physico-chemical characterization of Acticoat Flex3™ and *in vitro* release experiments of Ag and AgNPs from the product have been carried out in previous works.[22,41–43] Additional analyses performed in this study included the determination of pH-dependent colloidal stability and size distribution of primary NPs released from the dressing in water, and the identification of Ag-binding proteins in a synthetic serum substitute as the release medium. Fragments of the intact dressing (~130 mg) were placed into 6 mL of ultrapure water at pH adjusted to 5, 6 and 7 (using NaOH), and then sonicated for 16 min at 37% amplitude in an ice bath using a Q700 device (Qsonica, Newtown, CT, USA), equipped with microtip probe. The suspensions were centrifuged at 120 g for 10 min to settle major debris, and the supernatants were analysed to determine the ζ-potential by electrophoretic light scattering (ELS), and the size distribution by dynamic light scattering (DLS), using a Zetasizer Nano ZS system (Malvern Panalytical, Malvern, UK). For the identification of Ag-binding proteins in human serum substitute (HSS, from Steamcell Technologies, Vancouver, Canada), release experiments were carried out as reported previously.[42] After 72h of incubation with the dressing, 0.5 mL of HSS were purified from non-protein species and concentrated using a 3kDa cut-off centrifugal filter (Microcon Merck Millipore, Milan, Italy). Five μL of the solution recovered from the filter were diluted 100-fold in trifluoroacetic acid 0.1% vol. solution (in H_2O/acetonitrile 1:1 vol.), then 1 μL of the mix was deposited onto the appropriate sample holder and let dry. Analysis by matrix-assisted laser desorption time-of-flight mass spectrometry (MALDI-TOF-MS) was performed using an instrument Ultraflex II (Bruker Daltonics, Bremen, Germany) with pulsed UV laser beam (nitrogen laser, 337 nm) and operating in linear positive ion mode. External mass calibration was performed using the Protein Calibration Standard II (Bruker Daltonics), based on the average values of $[M+H]^+$ of trypsinogen, protein A, bovine serum albumin (BSA) and the average values of $[M+2H]^{2+}$ of protein A and BSA.

2.2 Patients recruitment

The study was carried upon approval by the Ethics Committee for Clinical Practice of the University Hospital of Padua (Prot. 28289/2016), and in accordance with the Declaration of Helsinki ethical guidelines, practice guidelines, and local laws and regulations. Informed written consent was obtained from all participants. The study involved four patients (A-D) providing skin samples through the bio-bank of the University Hospital of Padua. Patients were eligible for the study if affected by partial or full thickness burn or equivalent wound. All patients were treated at the Burns Centre of the Hospital, by using the same type of AgNPs-containing dressing as reported elsewhere,[22] and following current protocols without any additional invasive procedure. Beside eligibility criteria, patients were selected so to be representative of different protocols used for wound treatment, and distinct healing progressions, outlined below. Given the intrinsic

constrains, a relatively low number of patients and samples were selected for the analyses, and therefore must be considered within the specificity of their respective case-study.

Patient A (male, age 63) had partial thickness bilateral burn on the legs and hands, due to backfiring in an open environment. Biopsies were performed on deep partial thickness wound regions of the right leg. The first sample was collected after surgical cleaning of the wound and before a single application of the dressing, which was kept on site after complete healing. Further biopsies were performed at 3, 6, 9 and 12 days of treatment, corresponding to complete healing, from regions of interests at the wound margins above the dressing. Patient B (male, age 54) was affected by a degloving injury of the left leg, equivalent to a full thickness burn lesion. The first sample was collected after surgical cleaning of the wound and before application of the dressing. At 4, 7 and 10 days of treatment (complete healing) the dressing was changed, and biopsies were performed contextually. Patient C (female, age 56) had a full thickness flame burn to the thorax. The first sample was collected from the left axilla after surgical cleaning and before application of the dressing. Two additional biopsies were performed on the same area after 7 and 15 days of treatment in correspondence with dressing changes. At last sampling time, wound healing was still incomplete. Patient D (male, age 48) had a partial thickness flame burn to both legs and arrived in the Burns Centre after emergency treatment with Ag sulfadiazine 1% cream in another hospital. The first biopsy was performed on the medial region of the right leg, after application of the cream and before surgical cleaning, and a second biopsy after 5 days of treatment with a single application of the dressing, when skin regeneration was still incomplete.

2.3 Biopsy samples collection and preparation

Full-thickness biopsy samples of the wounds were collected using a surgical punch of 4 mm i.d. and 7 mm of length. The samples were immediately frozen at -80°C without any preserving or fixing agent. Despite this approach could induce minor morphological artifacts in the tissue due to the growth of ice crystals,[44] undetected in the histological analysis of these samples, it was selected as the most reliable to maintain the distribution and speciation of Ag.[45] Based on preliminary analyses, specific patients and samples were selected to be dedicated to semi-quantitative imaging or speciation analysis with optimized respective preparation procedures, in order to maximize the probability to extract useful and representative results. For LA-ICP-MS analysis, the samples were cryosectioned longitudinally into 20 µm thick slices. The sections were deposited onto uncoated microscope glass slides and dried at room temperature overnight. The residual unsliced portion of the samples from patient B was used for quantitative Ag determination by bulk ICP-MS analysis (see below). For SR-µXRF and SR-µXANES analyses, the samples were cryosectioned into slices of 30 µm of thickness, placed between Ultralene covered microscopy slices, and freeze-dried overnight. Histological images were obtained for slices (thickness 20 µm, ethanol stain followed by toluidine blue stain) adjacent to those that were analysed for elemental mapping and speciation.

2.4 Synchrotron radiation µXRF and µXANES

High-resolution imaging of Ag distribution and single-point speciation of the metal in the skin profiles of patient A were determined by SR-μXRF and Ag L_{III}-edge SR-μXANES analyses, respectively. The measurements were performed using the scanning X-ray microscope of beamline ID21, at the European Synchrotron Radiation Facility (ESRF, Grenoble, France), operating in a vacuum at room temperature. Details on the instrumental parameters are provided elsewere.[42] Whole-profile SR-μXRF imaging of Ag was performed in fluorescence mode with 3.42 keV of excitation energy, with a step (pixel) size of 2 μm and integration time of 100 ms, whereas localized maps of regions of interest were obtained at 3 to 0.5 μm pixel size. Other elements including P, S and Cl were also determined in all analyses to obtain structural information on the specimens. The raw data (counts) were elaborated using the software PyMca 4.7 (ESRF) as reported elsewhere[42] with some modifications. The SR-μXRF maps also provided a reference for spot selection of points of interest to collect Ag L_{III}-edge SR-μXANES spectra in the 3.32 to 3.42 keV energy range with 0.5 eV steps. The spectra were elaborated and finally treated by linear combination fitting (LCF) using the software Athena 0.9.24 as reported elsewhere.[42] Solid-state reference compounds used as input variables included: metallic Ag foil, AgCl, Ag_2SO_4, $AgNO_3$, Ag_2O, Ag sulfadiazine and a fragment of intact Acticoat Flex3™ dressing. Reference standards of metallic AgNPs of 10 nm nominal size, as citrate-stabilized water suspensions, were purchased from Sigma-Aldrich (Milan, Italy) and characterized for size distribution and colloidal stability as reported elsewhere.[42] A standard of Ag bonded to glutathione (GSH) was prepared by incubating ionic Ag in an aqueous solution of reduced L-glutathione (Sigma-Aldrich, Milan, Italy) at 37 °C under gentle shaking for 2h and in dark conditions, and freeze dried.

2.5 Laser ablation ICP-MS

The semi-quantitative distribution of Ag in the skin profiles of patients B-D was determined by LA-ICP-MS imaging analysis. The samples from patient B were analysed at the University of Aberdeen using a New Wave 213 UP system (Fremont, CA, USA) equipped with a standard cell and coupled to an ICP-MS model 7500c from Agilent Technologies (Tokyo, Japan). The samples from patients C and D were analysed at Ca' Foscari University of Venice using a LSX-213 $G2^+$ system (Teledyne CETAC Technologies, Omaha, Nebraska, USA), equipped with a solid-state laser based on a YAG crystal doped with Nd ($Nd:Y_3Al_5O_{12}$) and a HelEx™ two-volume cell, coupled to an ICP-MS model 7500cx from Agilent Technologies (Tokyo, Japan). All analyses were carried out in scan line mode with instrumental parameters optimized for a complete ablation of the tissue. The lateral resolution ranged between 4 and 24 μm, and the vertical resolution between 12 and 100 μm, depending on the map. Silver was measured by monitoring both m/z 107 and 109 (as an internal consistency check), but final elaborations were based on the former mass. Carbon (m/z 13) and P (m/z 31) were also measured in all analyses to get structural information on the specimens, while Zn (m/z 67) was measured to investigate possible correlation with Ag dynamics. The raw data (counts) were elaborated using the software PyMca. Low-resolution quantitative determination of the Ag content in the same samples collected from patient B was performed as reported elsewhere.[22] Briefly, the residual samples after cryosectioning were cut manually using a scalpel, digested overnight in an alkaline tetramethylammonium hydroxide solution at 60 °C, diluted in Triton X-100 0.1% vol. and NH_4OH 2.8% vol. aqueous solutions, and analysed using the Agilent

7500cx ICP-MS. High-resolution semi-quantitative concentration profiles for patient B were then calculated assuming that the mass-weighted average concentration of the low-resolution profiles was representative of (coincided with) the total concentration in the corresponding slice analysed by LA-ICP-MS. The average median signal intensity along the whole profile was calculated and represented against the corresponding known bulk concentration of Ag to obtain a calibration curve (Supplementary Fig. S1), then used to convert the distribution statistics of signal intensity into a mass concentration. Statistica 10 (Statsoft) and Office Excel 365 (Microsoft Corporation) were used for data elaboration and graphical works.

3 Results

3.1 Characterization of the dressing and release of Ag *in vitro*

According to the producer, Acticoat Flex3™ consists of polyester fibres coated with nanocrystalline Ag. From a previous characterization by scanning electron microscopy - energy dispersive X-ray spectroscopy (SEM-EDX)[43] (see also Supplementary Fig. S2A-C), the fibres are ~16 µm wide and homogeneously coated by a 1.6±0.3 µm thick layer of uncapped unoxidized metallic Ag with nanostructured features approximatively of 20 to 170 nm in size. To establish if the features are due to nano-roughness of a solid layer or weakly bound particles/agglomerates, the dressing was sonicated in water at pH 6 and 7, and analysed by DLS. As shown in Fig. S3, primary particles with a mean size of 14±3 nm were observed, in the form of a moderately polydisperse (polydispersity index -PDI- <0.4) and moderately stable (ζ-potential <-30 mV) suspension. At pH 5, partial oxidative dissolution leaded to size reduction (mean 10±3 nm) and increased colloidal stability (ζ-potential ~-43 mV).

The dressing was incubated in standard HSS, containing human serum albumin (HSA), transferrin (HTF) and recombinant insulin (HINS) in Iscove's Modified Dulbecco's Medium. As shown in Fig. 1, MALDI-TOF-MS spectra of the soluble Ag fraction revealed that HSA and HTF were bound respectively to 1 and 2 atoms of Ag per mole of protein (no mass shift was noticed for HINS, not shown). The final concentration of soluble Ag measured by ICP-MS was 0.98±0.03 mM, in good correspondence with the saturation of HSA (0.78 mM) and HTF (0.03 mM) given the found stoichiometry. The overall depletion of the coating after 3-days of static *in vitro* migration is minimal; most of the coating keeps attached to the fibers and residual detached agglomerates are still present in the medium, preserving the original nanostructured surface (Fig. S2C).

3.2 Spatiotemporal and structural distribution of Ag *in vivo* during a single application

Patient A was treated with a single application of the dressing until complete healing (12 days), allowing us to investigate the kinetics of Ag distribution in the healing wound. The samples were analysed by SR-µXRF to achieve a complementary detailed structural characterization of the specimen.

Before the first application of the dressing, the wound of patient A exhibited complete destruction of superficial skin layers (epidermis is absent), and thermal damage to the full thickness of the dermis (Fig. 2A and Supplementary Fig. S4A). This structure is typical of inflammation, the first

phase of wound healing, consisting in the formation of fibrin cloth and the massive release of signalling molecules for immune cells recruitment.[46] No Ag signal was observed in the whole profile of the skin by SR-μXRF (Supplementary Fig. S4C), supporting the absence of significant background levels or contamination of the sample.

After 3 days of treatment, the wound of patient A presented patchy missing and regenerating epidermis, and histological features typical of the proliferative phase (second phase of wound healing),[46] as shown in Fig. 3A, B. Where present, the stratified structure of the epidermis is well discernible from the distribution of P, S, and Cl (Fig. 3C, D). The high level of S in the surface layer (stratum corneum) is representative of the local accumulation of keratine, an insoluble fibrous protein with high proportion of the S-containing amino acid cysteine.[47] The distribution of P correlates with the cellular density (as a component of membrane phospholipids) and metabolic activity (from mitochondrial adenosine triphosphate -ATP- metabolism), both higher in the basal layer of the epidermis (stratum basale),[48] where proliferating cells provide new tissue for reconstruction of the upper layers.[49] Wide areas of highly vascularized granulation tissue, including islands of squamous epithelium, extend from the epidermis down to the deep dermis (reticular dermis). The granulation tissue forms during the proliferative phase of wound healing by an intensive and loosely organized production of new extracellular matrix (ECM), a network of glycoproteins, collagen and elastin fibres, that provides structural support to the dermal layer.[46] Below the granulation tissue, the reticular dermis presents as an organized and more dense structure of connective fibres, where Cl shows its highest concentration.[48,50] Hypodermis (large fat reservoirs crossed by connective fibres), can be observed at the bottom of the profile. Silver was present in significant levels with specific localization in the granulation tissue. The metal did not permeate the regenerating epidermis, the reticular dermis, and the underlying hypodermis. The zoom map in Fig. 3E shows that Ag formed irregular clusters in the granulation tissue at the edge of squamous epithelium, without penetrating it.

Six days after application of the dressing, the wound of patient A was still presenting middle areas that lacked the epidermal layer and was covered by an extended scab, as can be seen in Fig. 2B and in Fig. 4A-C. The histopathology and elemental maps of the skin profile (Fig. 4A and Supplementary Fig. S5A-C), are similar to the 3 days sample (Fig. 3A, C), with granulation tissue transitioning toward the deep dermis and an increasing density of connective fibres along the depth profile. The scab had the highest local level of Ag detected in all samples from this patient (Fig. 4D-F and Supplementary Fig. S5D) and was selected for further speciation analysis by SR-μXANES (see next section), but the metal was undetectable in the skin layers below (Supplementary Fig. S5C). The sample collected from the wound after 9 days of treatment had also very similar structural features and elemental distributions, except for the absence of the scab and Ag, correspondingly (Supplementary Fig. S6).

After 12 days, the wound reached complete healing (Fig. 2C) and had a fully structured histological profile (Fig. 5A, D). The elemental maps (Fig. 5E, F) show a dense and organized structure of the tissues. The epidermis presents a uniformly high level of P along the stratum basale and stratum spinosum, and a solid stratum corneum with predominant localization of S and Cl. The dermal

layer is also fully structured (Fig. 5B), showing an increasing density and organization of the ECM from the upper papillary layer to the deeper reticular layer, well represented by the increase of Cl. An arterial vessel is clearly visible in the lower part of the reticular dermis (Fig. 5C), just above the spongy hypodermis, with relatively high levels of P and S due to the high cellular density, but no significant traces of Ag. Silver was not detected along the whole skin profile, except for an individual particle ~7 µm in size located in the reticular dermis (Fig. 5G, H, corresponding to the SR-µXRF spectrum in Fig. 5I).

3.3 Semi-quantitative spatiotemporal distribution of Ag *in vivo* during repeated applications

Patient B was treated with repeated applications of the dressing until complete healing (10 days), which is the most used therapeutic approach. Laser ablation ICP-MS analysis was adopted to focus the study on the semi-quantitative aspects of Ag accumulation.

The spatiotemporal distribution of Ag, Zn, P and C in the healing wound of patient B, obtained by LA-ICP-MS imaging, is shown in Fig. 6A. The maps of P and C enable us to identify the raw structural characteristics of the specimen (see also Fig. 7). High levels of C in the lower profile outline the location of hypodermis, whose adipose tissue is enriched in triglycerides,[51] while P is more concentrated in the epidermis and the wall of blood vessels, as observed by SR-µXRF in the profiles from patient A. After the first application of the dressing, the penetration of Ag into the tissue was extensive and consistent with that observed for patient A, reaching a depth of ~1.5 mm into the granulation tissue. Repeated applications of new dressings entailed further release and accumulation of Ag in the skin, with a progressively patchier distribution along the profile. High levels of the metal characterize the papillary dermis even after complete healing. A detailed map of the healed wound's upper profile (Fig. 6B) shows that Ag was not detected in the regenerated epidermis, although clusters of the metal persist in the dermis above. Thick deposits of Ag on the surface of the stratum corneum confirm that the metal is released from the dressing also over the regenerating/intact epidermis, but is unable to penetrate the skin barrier, as previously hypothesized from indirect estimations.[43]

Quantitative analysis by ICP-MS after mineralization of the biopsy residues provided low-resolution but highly accurate profiles of Ag mass concentration (Fig. 6C), from which average full-profile levels of 8.4, 3.9 and 6.3 ng mg^{-1} were obtained for the wound after 3, 7 and 10 days, respectively. Silver reached the highest concentration within the first mm of depth, at between 10 and 31 ng mg^{-1}, corresponding to 0.38-0.75 µg *per* cm^{-2} of the dressing. After application of a semi-quantitative calibration, the elemental maps of Ag were converted into high-resolution concentration profiles, less accurate than bulk levels, but providing information on the relative spatial dispersion of Ag at the micrometric scale. The semi-quantitative high-resolution profiles (Fig. 6C) are consistent with quantitative data and confirm a considerable lack of homogeneity in the metal spatial distribution at the micrometric scale, with regions of accumulation in the granulation tissue, where Ag reaches a maximum level of 614 ng mg^{-1} (3 days profile).

According to the maps in Fig. 6A, Zn exhibits a relatively uniform distribution in the wound before treatment, but localized deposits of this metal were detected in the adipose tissue 4 days

afterwards. A further and more homogeneous increase in Zn levels in the hypodermis was observed after 7 days, accompanied by a slightly higher concentration in the regenerating epidermis compared to the dermis. In the healed skin, Zn levels and distribution in the dermis and hypodermis reverted to those in the initial stage, but still showing relatively higher levels in the epidermis, as previously documented.[52]

Multiple applications of the dressing were adopted also for patient C, who did not exhibit a successful regeneration of the tissues after 15 days of treatment. The imaging data of the 15 days profile obtained by LA-ICP-MS (Fig. 7) mark a significant accumulation of Ag in the granulation tissue, comparable to that of patient A after 4 days of treatment. In the adipose tissue, oblique sections of two blood vessels show characteristic elemental compositions. The vein vessel above has an irregular section with thin walls and high levels of P, low levels of Zn, and undetected levels of Ag. The lower arterial vessel has significant concentrations of Ag in the internal lamina, compared to its absence in the surrounding tissue. Conversely, high levels of P and Zn were detected in the thick wall of arterial vessel.

Differently to the others, patient D underwent emergency treatment with Ag sulfadiazine before application of the dressing. The maps of Ag distribution along the skin profiles before the first application of the dressing and 5 days after (Supplementary Fig. S7) show penetration and distribution of the metal globally comparable to those observed for the other patients during the proliferative phase, with a significant increase of surface Ag level after application of the dressing.

3.4 Semi-quantitative speciation of Ag *in vivo*

Preliminary SR-μXANES analyses performed on the intact dressing confirmed previous observations,[22,36,53] whereby AgNPs are released by the dressing into the wound environment mainly as aggregates/agglomerates (in terms of molar fraction), whose SR-μXANES spectra are more similar to that of Ag^0 foil rather than to metallic AgNPs suspended standards.

Based on the high Ag level detected in SR-μXRF maps, regions of the same specimens from patient A were selected for SR-μXANES speciation analysis. They included: one spot in the dermis of the 3 days specimen (marked in Fig. 3E and with the SR-μXRF spectrum in Fig. 3F), and five spots in the scab of the 6 days specimen (marked in Fig. 4E, F), the latter drawing a depth transect. The corresponding average SR-μXANES spectra are represented in Fig.s 3G and 4G. Other regions within the same samples were explored without obtaining sufficient signal for reliable speciation analysis. Identification of the Ag species and semi-quantitative estimation of their relative molar fraction were achieved by LCF using the spectra of pure standards as reported in the Methods. The results (see Fig. 4H and Supplementary Table S1) depict a gradual change of speciation as we went deeper into the scab, possibly corresponding to specific spatiotemporal dynamics, whose endpoint is represented by the speciation of Ag in the dermis of the 3 days sample. Intact metallic AgNPs were detected in the scab tissue accounting for ~30% of total Ag in the upper 15 μm, decreasing to 16% at 30 μm depth and disappearing at 45 μm. However, the main species of Ag on the surface was the chloride complex, starting from ~60% of total Ag in the upper 45 μm, reaching 73% at 45 μm, then decreasing to 32% at 55 μm to disappear at 500 μm of depth into

the dermis. These changes were accompanied by a complementary increase in the Ag-protein thiol complexes, which started to be detectable at 30 µm until it became the only identifiable species in the dermis (molar fraction 81%). The speciation of Ag in the sixth spot of Fig. 3F was comparable to that of the scab surface, showing that micrometric agglomerates of pristine metallic NPs can be eventually embedded in deeper layers of the scab, but undergo the same transformations of the metal.

4 Discussion

Amongst the Ag-containing wound dressings, Acticoat Flex3™ is one of the most widely used. The dressing is intended for use on first to second degree burns and chronic ulcers. It is applied directly onto the wound, eventually moistened with drinking water in the absence of exudate and secured with a gauze. Even if the antibacterial effect is declared for up to 3 days, direct experience in the Burn Center has shown that the application time may be considerably varied to optimize the efficacy based on the specific conditions of each wound.

According to both producer specifications and independent characterization, the dressing consists of polymer fibres homogeneously coated by a layer of uncapped unoxidized metallic AgNPs. We observed that primary particles in the size range of 10 nm can be potentially released as isolated objects and kept relatively stable in a liquid medium, particularly at the slightly acidic pH typical of wound fluids. Still, under realistic *in vitro* conditions they are mainly released as agglomerates and in such form undergo surface chemical transformations resulting in final release of Ag(I) species, more rapidly than possible deagglomeration of the bulk metallic core.[42] These mechanisms strongly limit the local mobility of AgNPs, and make dissolution the driver for Ag mobility and bioaccessibility into the wound.

Another important variable in release scenarios is concentration, which could compensate for the potentially limited mobility of AgNPs for dynamic reasons. Silver concentration in the intact product is high: 119±2 mg g^{-1} corresponding to 0.822±0.016 mg cm^{-2}.[43] A previous study has shown that only ~7% of the Ag is released as dissolved species from 0.3 g of dressing in a 100-fold larger mass of HSS after 72h of static incubation.[41] Still, from analysis of the dressing after use *in vivo*, the estimated actual release into the patient's tissues was considerably higher, ranging from 28% to 62% of such a dose.[43] Locally, the release is strictly dependent on the characteristics of the wound bed, being much higher in presence of serous and purulent exudate.[43] The values above indicate a minimum dosage of 230 µg cm^{-2} as Ag administered to the patient, which amounts to more than double the maximum concentration applied until now in all studies evaluating the *in vitro*/*ex vivo* permeation of liquid suspended AgNPs through human or porcine skin (min 0.34, max 113 µg cm^{-2}).[32–34,53,54] The lack of a realistic reference dosage for such experiments limits their comparability. This is also exacerbated by the short exposure times (24h) and the static experimental conditions, compromising the reliability of the absolute permeated levels of Ag.

Relative evaluations of the available literature data support the hypothesis of a strong correlation between the penetration ability of AgNPs and the level of structural damage to the skin barrier,[34,53] suggesting extensive translocation of the metal into wounded tissues. In the skin of a

real patient, treated with a triplicate application of the AgNPs-containing dressing, we measured a maximum concentration of Ag in the range of 10-31 ng mg^{-1} (0.38-0.75 µg cm^{-2}). These values are significantly higher than the maximum levels estimated *in vitro* for AgNPs (coated with polyvinyl pyrrolidone -PVP-) in glycerolized dermis (3.5 ng mg^{-1}),[53] but compatible with the *in vitro* penetration of uncapped AgNPs in cryopreserved intact epidermis (mode 1.05 µg cm^{-2}) and dermis (mode 0.30 µg cm^{-2}).[54] Highly variable total levels of Ag have been previously observed *in vivo*, in healthy (range 6 to 199 ng mg^{-1} after one application,[36] and burnt tissues (range 9.1 to 47.5 ng mg^{-1} after max two applications;[22] 136±91 ng mg^{-1} after nine applications[40]), when the dressing was applied to humans or pigs under simulated conditions.

In the present study, it was shown that single-status bulk data are not comparable, because the level of Ag in the wound is highly dependent on the time, space (depth), and on the local structural characteristics of the tissue.

High-resolution two-dimensional maps of Ag distribution confirmed the previous observations from low-resolution depth profiles,[22] namely that Ag can significantly penetrate the skin of burn patients at the millimetre scale down to the dermis, which is considerably deeper than previous observations *in vitro*/*ex vivo* for intact or tape-stripped porcine skin (max 22±5 µm).[32,33] The characteristic spatiotemporal distribution of the metal in the wound tissue suggests an inverse association with its level of structural organization, as Ag penetrates rapidly and in depth only into the granulation tissue. As the skin regenerates, the metal accumulates in the upper layers of the dermis, while its concentration in the deeper layers decreases, supporting an efficient process of clearance. Local persistence of Ag was noticed only in patchy accumulation regions, where a structured organization of the collagen fibres was still lacking and/or due to the possible translocation of the metal from adjacent unhealed zones. On a clinical basis, no interference was observed on the process of wound healing after treatment with the AgNPs-containing dressing. The distribution pattern of Ag is therefore likely to be a consequence, not a cause of the structural characteristics of the tissue. As long as the regeneration proceeds correctly and new epidermis is formed, further AgNPs released by the dressing are unable to penetrate the stratum corneum. The kinetics of Ag clearance in a regularly healing wound after a single application of the dressing, shows that after 12 days the metal is almost quantitatively removed from the skin.

The spatio-temporal distribution of total Ag in the wounded skin provides only partial depicting of its dynamics, complemented by biochemical transformations. Several studies have investigated the dissolution kinetics of functionalized AgNPs *in vitro* using a medium whose maximum complexity consisted of cell culture media (Dulbecco's Modified Eagle Medium and Hoagland's Modified Medium).[14] They showed that organic molecules slow down the process by surface passivation, while chloride accelerates it, and helps the formation of secondary particles. Pooled with a complementary study recently carried out *in vitro*,[42] the present data on Ag speciation in wound tissues suggest an integrated and space/time-dependent process taking place at first on the surface of the pristine metallic aggregates of NPs. In contact with the acidic wound fluids Ag^{+} ions are released and rapidly transformed into a crust of insoluble chlorides (kinetically favoured) at the agglomerates' surface, these are then coated by a protein corona. As penetration of AgNPs

proceeds into the wound (in time at a daily scale, and in space at the tenth of µm scale), the metal is exchanged between chloride and protein thiols that are more thermodynamically favoured complexing agents. Protein complexes are the quantitatively dominant form of Ag into the skin tissues, and the responsible for mobilization of the metal towards vascular networks, resulting in its final removal from the wound. In patient C, who underwent multiple applications of the dressing for 15 days without full healing, we observed a significant level of Ag in the wall of an arterial vessel, while the metal was absent in the surrounding tissue. This supports an extensive systemic mobilization of Ag within the bloodstream, beside local permeation into the wound, compatibly with previous quantitative data on Ag levels in the blood of burn patients.[42]

As argued by simplified *in vitro* simulations,[41] this *in vivo* observation indicates that serum proteins in the contact medium play a central role as the driving factor for the kinetics of a set of concatenated processes, including: i) release of Ag from the dressing; ii) dissolution of the particles; and iii) mobilization of Ag^+ through the skin and the vascular system. In the exudate, and other intercellular environments several bioligands may be responsible for Ag binding through R-SH groups, including HSA, immunoglobulin G,[55] GSH[56], metallothioneins (MTs)[57,58] and HTF, as observed here. At the surface of AgNPs, such interactions affect their dissolution rate and agglomeration state in protein-specific ways.[55] Given the abundance and the colloidal stabilization action, HSA is a major candidate for passive carriage of Ag in both nanoparticulate and ionic from. Notably, the formation of protein corona and sequestration of Ag^+ by thiol groups in the extracellular fluids affect the cellular uptake of Ag, impacting its cytotoxicity, and reduce its antimicrobial efficacy, as shown against *E. coli*, *P. aeruginosa* and *S. aureus*.[56]

In any case, the clearance of Ag from the skin of patient A involved in this study required dissolution and protein complexation, and is compatible with the absence of AgNPs agglomerates in the blood of other burn patients treated with the same dressing.[42] Persisting Ag deposits were observed in the dermis after repeated applications of the dressing, which were supposed to be pristine agglomerates of AgNPs mechanically inserted into the open wound during the first phase of treatment, and are sufficiently large to have slower dissolution compared to the surrounding regeneration of the tissue.[59] This scenario is more probable than formation of secondary particles of sulphide/selenide complexes (which have been proposed to occur in the gastrointestinal tract)[9] or photoreduced metallic Ag (since the wound is protected from light), and can also explain the localized cellular internalization of AgNPs agglomerates that was previously observed (see also Supplementary Fig. S2D-F).[22] Still, further investigations are needed to establish the composition of Ag species in such residual deposits of the metal. Similar dynamics were observed in the patient D pre-treated with Ag sulfadiazine. This supports the hypothesis that both AgNPs and Ag sulfadiazine share the same final mechanism of Ag mobilization into the skin through the Ag^+ complexed ion. The dissolution of AgNPs and further changes in speciation of the metal observed during penetration into the wound tissues *in vivo*, shows that the dynamics of total Ag cannot be considered as representative of that of AgNPs. This demonstrates that any quantitative skin permeation experiment carried out so far must be considered incomplete without a complementary speciation study, and that *in vitro* experiments are currently far from representing reliable simulations of a real wound environment.

In spite of the rapid clearance of Ag from the skin observed here, the metal can bind several ligands other than thiols, such as amino, carboxyl, phosphate and imidazole groups, making it prone to interfere with many intracellular systems, including RNA and DNA.[57] Particularly in the regenerating wound, the interaction of Ag with MTs, beside its own detoxification, may affect other key functions that these metalloenzymes play in the modulation of inflammatory response, formation of granulation tissue and the epidermal proliferation.[57] An altered homeostasis of Zn may mirror these effects. In the regenerating wound, Zn plays an important role as a cofactor of MTs, stabilizer of cellular membranes and up-regulator of mitotic processes.[39,57,61] It may also act as a modulator of matrix metalloproteinases (MMPs, proteolytic enzymes responsible for ECM degradation and reconstruction, and cell migration modulation),[62] and as an up-regulator of integrins (responsible for keratinization and keratinocytes migration)[63] and Zn-finger transcription factors. These actions can explain the increase in intracellular Zn levels observed in the regenerating wound, particularly during the early inflammation phase and at the wound margins.[58,61] Assuming that the distribution of Zn mirrors the activity or the expression of MTs, higher levels are expected in the epidermis than in the dermis both in healthy skin[61] and in regenerating wounds during the proliferative phase (2-5 days in a rat model).[62] The elemental maps obtained in this study confirm this hypothesis, showing higher levels of Zn in the epidermis than in the dermis both during regeneration, and after complete healing. A maximum increase of the overall Zn level was observed 7 days after injury, followed by a re-normalization after 10 days. However, the maps revealed the highest concentration and increase of Zn in the adipose tissue, which has not been documented before. We also observed relatively high levels of Zn in the wall of an arterial vessel. The latter may be representative of the role played by Zn in angiogenesis by modulating the activity of MMPs, or with normal expression of MTs in vascular endothelial cells,[64] and is compatible with the observed accumulation of Zn in the aorta of a rat model after intravenous injection of inorganic Zn.[65] An interaction between Ag and Zn should also be considered. Some authors suggest that Ag promotes epidermal cell proliferation by increasing the uptake of Zn and Cu through induction of MTs synthesis,[66] possibly mediated by intracellular ROS generation;[28] while others state that AgNPs are able to indirectly down-regulate the activity of MMPs in the wound,[67] resulting in dermal inflammatory cell apoptosis, possibly through the displacement of Zn^{2+} by the Ag^{+} ion.[68] We observed an opposite distribution of the two metals during healing. Combined with the dissolution of AgNPs in the exudate and the upper wound layers, this supports an interaction between Ag and Zn which is mediated by their ionic forms.

5 Conclusion

Our findings demonstrate that both SR-µXRF and LA-ICP-MS enable two-dimensional imaging of Ag (and multielemental) distribution in human tissues, with a comparable sensitivity of ~200 cps μm^{-2} *per* pg mg^{-1} of the metal. Synchrotron radiation-µXRF has a fixed spatial resolution determined by the size of the beam at the specific beamline (usually ≈1 x 0.5 µm at ID21), and is non-destructive, being perfectly suited to compare the distribution of Ag with the structural characteristics of the biological tissue. It also allows to perform point-specific speciation analysis of Ag by SR-µXANES, at the same micrometre scale. Still, LA-ICP-MS instruments have tunable beam size (from 5 to 200 µm for those used in this work), and high power, to improve the absolute

detection limit for Ag well below the level of ng mg^{-1}, over larger scanned areas. The advantages of these techniques were combined to achieve the first direct observation of the biochemical dynamics of Ag into full-profile specimens of wounded skin from four patients, treated with the dressing Acticoat Flex3™. Rapid release and accumulation of Ag onto the wound bed, and millimetre-scale penetration of the metal into the damaged tissues, were observed. Still, speciation data proved that, *in vivo* and in real patients, AgNPs get rapidly dissolved *in situ* before reaching the systemic distribution, while extensive mobilization of Ag involves its bio-complexed ionic species. These data support the capability of the dressing to exert an intense bioactive action focused onto the surface layer of the wound. Further applications of this experimental approach to a wider number and variety of patients, wounds, samples and dressings will be important to strengthen the representativity of present results in realistic clinical scenarios. Questions remain open on the effects of possible functionalization of AgNPs in alternative dressing designs, the biochemical mechanisms and clinical relevance of possible toxic effects leaded by the metal during its residence time into the wound, the mechanisms of potential interaction with Zn, and the fate of Ag after entering systemic circulation.

Conflict of Interest

The authors declare that the research was conducted in the absence of any commercial or financial relationships that could be construed as a potential conflict of interest.

Author Contributions

MR. was the Principal Investigator of the ESRF project; WRLC was the Principal Investigator of the overarching FIRB project. MR, CR and WRLC performed the analyses, the main laboratory work and manuscript elaboration. HC-M contributed to the measurements at the ESRF; DU and JF contributed to the LA-ICP-MS analyses at the University of Aberdeen; IM and VV collected the samples and provided clinical data; IM, FB contributed to the samples preparation; CB provided scientific and coordination support.

Funding

This research was supported by funds from the MIUR-FIRB project number RBFR08M6W8.

Acknowledgments

ELGA LabWater is acknowledged for providing the PURELAB Option-Q and Ultra Analytic systems, which produced the ultra-pure water used for Ag determinations. Adam Douglas and Dhinesh Asogan are acknowledged for their technical support during LA-ICP-MS analysis at the University of Venice, and the authors gratefully acknowledge Bill Spence and Teledyne Cetac Technologies for the loan of the laser ablation instrumentation. Laura Molin and ISTM-CNR are acknowledged for MALDI-TOF-MS analysis. The synchrotron experiments were performed on beamline ID21 at the European Synchrotron Radiation Facility (ESRF), Grenoble, France (proposal #CH4121).

References

1 Y. K. Coban, *World J. Crit. care Med.*, 2012, **1**, 94–101.

2 M. P. Rowan, L. C. Cancio, E. A. Elster, D. M. Burmeister, L. F. Rose, S. Natesan, R. K. Chan, R. J. Christy and K. K. Chung, *Crit. Care*, 2015, **19**, 243.

3 D. J. Barillo and D. E. Marx, *Burns*, 2014, **40**, S3–S8.

4 M. A. Ansari, H. M. Khan, A. A. Khan, S. S. Cameotra and M. A. Alzohairy, *Indian J. Med. Microbiol.*, 2015, **33**, 101–9.

5 J. P. Sterling, *Burns*, 2014, **40**, S19–S23.

6 M. Rai, A. Yadav and A. Gade, *Biotechnol. Adv.*, 2009, **27**, 76–83.

7 D. R. Monteiro, L. F. Gorup, A. S. Takamiya, A. C. Ruvollo-Filho, E. R. de Camargo and D. B. Barbosa, *Int. J. Antimicrob. Agents*, 2009, **34**, 103–110.

8 S. Chernousova and M. Epple, *Angew. Chemie Int. Ed.*, 2013, **52**, 1636–1653.

9 J. Liu, Z. Wang, F. D. Liu, A. B. Kane and R. H. Hurt, *ACS Nano*, 2012, **6**, 9887–9899.

10 S. Ahlberg, A. Antonopulos, J. Diendorf, R. Dringen, M. Epple, R. Flöck, W. Goedecke, C. Graf, N. Haberl, J. Helmlinger, F. Herzog, F. Heuer, S. Hirn, C. Johannes, S. Kittler, M. Köller, K. Korn, W. G. Kreyling, F. Krombach, J. Lademann, K. Loza, E. M. Luther, M. Malissek, M. C. Meinke, D. Nordmeyer, A. Pailliart, J. Raabe, F. Rancan, B. Rothen-Rutishauser, E. Rühl, C. Schleh, A. Seibel, C. Sengstock, L. Treuel, A. Vogt, K. Weber and R. Zellner, *Beilstein J. Nanotechnol.*, 2014, **5**, 1944–65.

11 A. B. G. Lansdown, *Silver in Healthcare*, Royal Society of Chemistry, Cambridge, 2010.

12 D. L. Hashmi and L. Haith, *Curr. Trauma Reports*, 2019, **5**, 160–168.

13 H. . Klasen, *Burns*, 2000, **26**, 131–138.

14 K. Loza, J. Diendorf, C. Sengstock, L. Ruiz-Gonzalez, J. M. Gonzalez-Calbet, M. Vallet-Regi, M. Köller and M. Epple, *J. Mater. Chem. B*, 2014, **2**, 1634.

15 C. You, C. Han, X. Wang, Y. Zheng, Q. Li, X. Hu and H. Sun, *Mol. Biol. Rep.*, 2012, **39**, 9193–9201.

16 O. Bondarenko, A. Ivask, A. Käkinen, I. Kurvet and A. Kahru, *PLoS One*, 2013, **8**, e64060.

17 N. Tra Thanh, M. Ho Hieu, N. Tran Minh Phuong, T. Do Bui Thuan, H. Nguyen Thi Thu, V. P. Thai, T. Do Minh, H. Nguyen Dai, V. T. Vo and H. Nguyen Thi, *Mater. Sci. Eng. C*, 2018, **91**, 318–329.

18 N. Masood, R. Ahmed, M. Tariq, Z. Ahmed, M. S. Masoud, I. Ali, R. Asghar, A. Andleeb and A. Hasan, *Int. J. Pharm.*, 2019, **559**, 23–36.

19 A. Mandal, S. Sekar, K. M. Seeni Meera, A. Mukherjee, T. P. Sastry and A. B. Mandal, *Phys. Chem. Chem. Phys.*, 2014, **16**, 20175–20183.

20 K. Kalantari, E. Mostafavi, A. M. Afifi, Z. Izadiyan, H. Jahangirian, R. Rafiee-Moghaddam and T. J. Webster, *Nanoscale*, 2020, 12, 2268–2291.

21 A. Adhya, J. Bain, O. Ray, A. Hazra, S. Adhikari, G. Dutta, S. Ray and B. K. Majumdar, *J. basic Clin. Pharm.*, 2014, **6**, 29–34.

22 C. Rigo, L. Ferroni, I. Tocco, M. Roman, I. Munivrana, C. Gardin, W. R. L. Cairns, V. Vindigni, B. Azzena, C. Barbante and B. Zavan, *Int. J. Mol. Sci.*, 2013, **14**, 4817–40.

23 N. S. Moiemen, E. Shale, K. J. Drysdale, G. Smith, Y. T. Wilson and R. Papini, *Burns*, 2011, **37**, 27–35.

24 E. Vlachou, E. Chipp, E. Shale, Y. T. Wilson, R. Papini and N. S. Moiemen, *Burns*, 2007, **33**, 979–985.

25 L. Nherera, P. Trueman, C. Roberts and L. Berg, *Wound Repair Regen.*, 2017, **25**, 707–721.

26 S. W. P. Wijnhoven, W. J. G. M. Peijnenburg, C. A. Herberts, W. I. Hagens, A. G. Oomen, E. H. W. Heugens, B. Roszek, J. Bisschops, I. Gosens, D. Van De Meent, S. Dekkers, W. H. De Jong, M. van Zijverden, A. J. A. M. Sips and R. E. Geertsma, *Nanotoxicology*, 2009, **3**, 109–138.

27 S. Ahlberg, M. C. Meinke, L. Werner, M. Epple, J. Diendorf, U. Blume-Peytavi, J. Lademann, A. Vogt and F. Rancan, *Eur. J. Pharm. Biopharm.*, 2014, **88**, 651–657.

28 P. V. AshaRani, G. Low Kah Mun, M. P. Hande and S. Valiyaveettil, *ACS Nano*, 2009, **3**, 279–290.

29 Z. Xiu, Q. Zhang, H. L. Puppala, V. L. Colvin and P. J. J. Alvarez, *Nano Lett.*, 2012, **12**, 4271–4275.

30 C. Graf, D. Nordmeyer, C. Sengstock, S. Ahlberg, J. Diendorf, J. Raabe, M. Epple, M. Köller, J. Lademann, A. Vogt, F. Rancan and E. Rühl, *Langmuir*, 2018, **34**, 1506–1519.

31 M. E. Samberg, S. J. Oldenburg and N. A. Monteiro-Riviere, *Environ. Health Perspect.*, 2010, **118**, 407–413.

32 Y. Zhu, C.-S. Choe, S. Ahlberg, M. C. Meinke, U. Alexiev, J. Lademann and M. E. Darvin, *J. Biomed. Opt.*, 2014, **20**, 051006.

33 A. Vogt, F. Rancan, S. Ahlberg, B. Nazemi, C. S. Choe, M. E. Darvin, S. Hadam, U. Blume-Peytavi, K. Loza, J. Diendorf, M. Epple, C. Graf, E. Rühl, M. C. Meinke and J. Lademann, *Beilstein J. Nanotechnol.*, 2014, **5**, 2363–73.

34 F. F. Larese, F. D'Agostin, M. Crosera, G. Adami, N. Renzi, M. Bovenzi and G. Maina, *Toxicology*, 2009, **255**, 33–37.

35 C. J. Coombs, A. T. Wan, J. P. Masterton, R. A. J. Conyers, J. Pedersen and Y. T. Chia, *Burns*, 1992, **18**, 179–184.

36 R. George, S. Merten, T. T. Wang, P. Kennedy and P. Maitz, *Australas. J. Dermatol.*, 2014, **55**, 185–190.

37 J. Liu, D. A. Sonshine, S. Shervani and R. H. Hurt, *ACS Nano*, 2010, **4**, 6903–6913.

38 D. M. Ansell, K. A. Holden and M. J. Hardman, *Exp. Dermatol.*, 2012, **21**, 581–585.

39 A. B. G. Lansdown, A. Williams, S. Chandler and S. Benfield, *J. Wound Care*, 2005, **14**, 155–160.

40 X.-Q. Wang, H.-E. Chang, R. Francis, H. Olszowy, P.-Y. Liu, M. Kempf, L. Cuttle, O. Kravchuk, G. E. Phillips and R. M. Kimble, *J. Cutan. Pathol.*, 2009, **36**, 788–792.

41 C. Rigo, M. Roman, I. Munivrana, V. Vindigni, B. Azzena, C. Barbante and W. R. L. Cairns, *Burns*, 2012, **38**, 1131–1142.

42 M. Roman, C. Rigo, H. Castillo-Michel, I. Munivrana, V. Vindigni, I. Mičetić, F. Benetti, L. Manodori and W. R. L. Cairns, *Anal. Bioanal. Chem.*, 2016, **408**, 5109–5124.

43 M. Roman, C. Rigo, I. Munivrana, V. Vindigni, B. Azzena, C. Barbante, F. Fenzi, P. Guerriero and W. R. L. Cairns, *Talanta*, 2013, **115**, 94–103.

44 A. Bullen, R. R. Taylor, B. Kachar, C. Moores, R. A. Fleck and A. Forge, *Hear. Res.*, 2014, **315**, 49–60.

45 M. J. Hackett, J. A. McQuillan, F. El-Assaad, J. B. Aitken, A. Levina, D. D. Cohen, R. Siegele, E. A. Carter, G. E. Grau, N. H. Hunt and P. A. Lay, *Analyst*, 2011, **136**, 2941–2952.

46 G. Broughton, J. E. Janis and C. E. Attinger, *Plast. Reconstr. Surg.*, 2006, **117**, 1e-S-32e-S.

47 P. N. Deo and R. Deshmukh, *J. Oral Maxillofac. Pathol.*, 2018, **22**, 86–91.

48 Y. Werner-Linde, J. Pallon and B. Forslind, *Scanning Microsc.*, 2004, **12**, 599–608.

49 D. D. Bikle, *Mol. Cell. Endocrinol.*, 2011, **347**, 80–89.

50 T. von Zglinicki, M. Lindberg, G. M. Roomans and B. Forslind, *Acta Derm. Venereol.*, 1993, **73**, 340–3.

51 D. S. Urgast, D. G. Ellingsen, B. Berlinger, E. Eilertsen, G. Friisk, V. Skaug, Y. Thomassen, J. H. Beattie, I.-S. Kwun and J. Feldmann, *Anal. Bioanal. Chem.*, 2012, **404**, 89–99.

52 E. D. Desouza, I. A. Atiya, A. Al-Ebraheem, B. C. Wainman, D. E. B. Fleming, F. E. McNeill and M. J. Farquharson, *Appl. Radiat. Isot.*, 2013, **77**, 68–75.

53 C. Bianco, G. Adami, M. Crosera, F. Larese, S. Casarin, C. Castagnoli, M. Stella and G. Maina, *Burns*, 2014, **40**, 1390–1396.

54 C. Bianco, S. Kezic, M. Crosera, V. Svetličić, S. Šegota, G. Maina, C. Romano, F. Larese and G. Adami, *Int. J. Nanomedicine*, 2015, **10**, 1899.

55 A. Sasidharan, J. E. Riviere and N. A. Monteiro-Riviere, *J. Mater. Chem. B*, 2015, **3**, 2075–2082.

56 G. Mulley, A. T. A. Jenkins and N. R. Waterfield, *PLoS One*, 2014, **9**, e94409.

57 A. B. G. Lansdown, *Wound Repair Regen.*, 2002, **10**, 130–32.

58 K. S. Vignesh and G. S. Deepe, *Int. J. Mol. Sci.*, 2017, 18.

59 W. Zhang, Y. Yao, N. Sullivan and Y. Chen, *Environ. Sci. Technol.*, 2011, **45**, 4422–4428.

60 P. D. Marcato, L. B. De Paula, P. S. Melo, I. R. Ferreira, A. B. A. Almeida, A. S. Torsoni and O. L. Alves, *J. Nanomater.*, 2015, **2015**, 1–10.

61 A. B. G. Lansdown, U. Mirastschijski, N. Stubbs, E. Scanlon and M. S. Ågren, *Wound Repair Regen.*, 2007, **15**, 2–16.

62 A. Michopoulou and P. Rousselle, *Eur. J. Dermatology*, 2015, **25**, 33–42.

63 I. Tenaud, S. Leroy, N. Chebassier and B. Dreno, *Exp. Dermatol.*, 2000, **9**, 407–416.

64 M. Iwata, T. Takebayashi, H. Ohta, R. E. Alcalde, Y. Itano and T. Matsumura, *Histochem. Cell Biol.*, 1999, **112**, 283–90.

65 D. S. Urgast, O. Ou, M.-J. Gordon, A. Raab, G. F. Nixon, I.-S. Kwun, J. H. Beattie and J. Feldmann, *Anal. Bioanal. Chem.*, 2012, **402**, 287–297.

66 A. B. G. Lansdown and A. Williams, *J. Wound Care*, 2004, **13**, 131–136.

67 J. B. Wright, K. Lam, A. G. Buret, M. E. Olson and R. E. Burrell, *Wound Repair Regen.*, **10**, 141–51.

68 H. Li and J. D. Otvos, *Biochemistry*, 1996, **35**, 13937–13945.

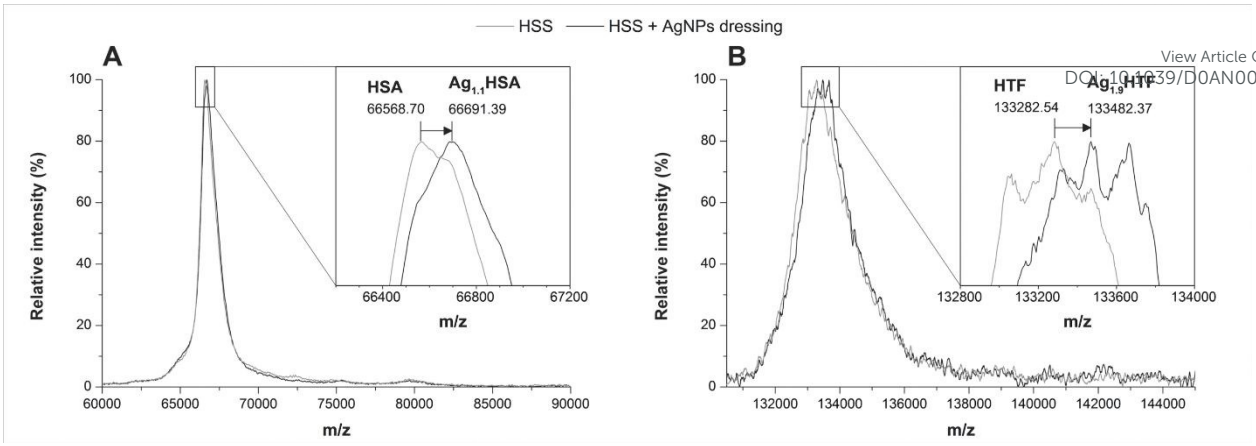

Figure 1. MALDI-TOF-MS spectra of selected m/z windows showing the peaks of HSA (A) and HTF (B) in HSS after 72h of static incubation of the AgNPs-containing dressing (black line), and corresponding control medium (gray line). The mass shifts corresponding to bounded Ag ions are indicated.

View Article Online
DOI: 10.1039/D0AN00607F

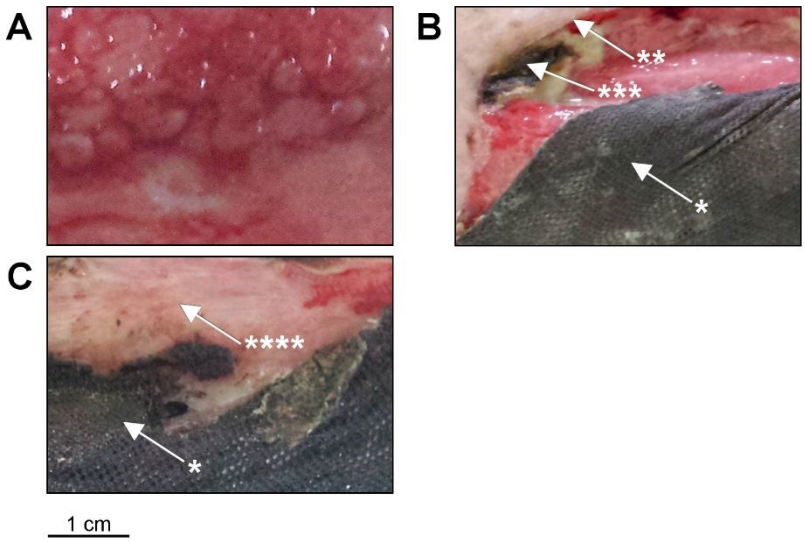

Figure 2. Pictures of the wound of patient A before application of the AgNP-containing dressing (A) and after 6 (B) and 12 (C) days of treatment. The arrows indicate: *dressing; **wound margin; ***scab; ****healed skin.

View Article Online
DOI: 10.1039/D0AN00607F

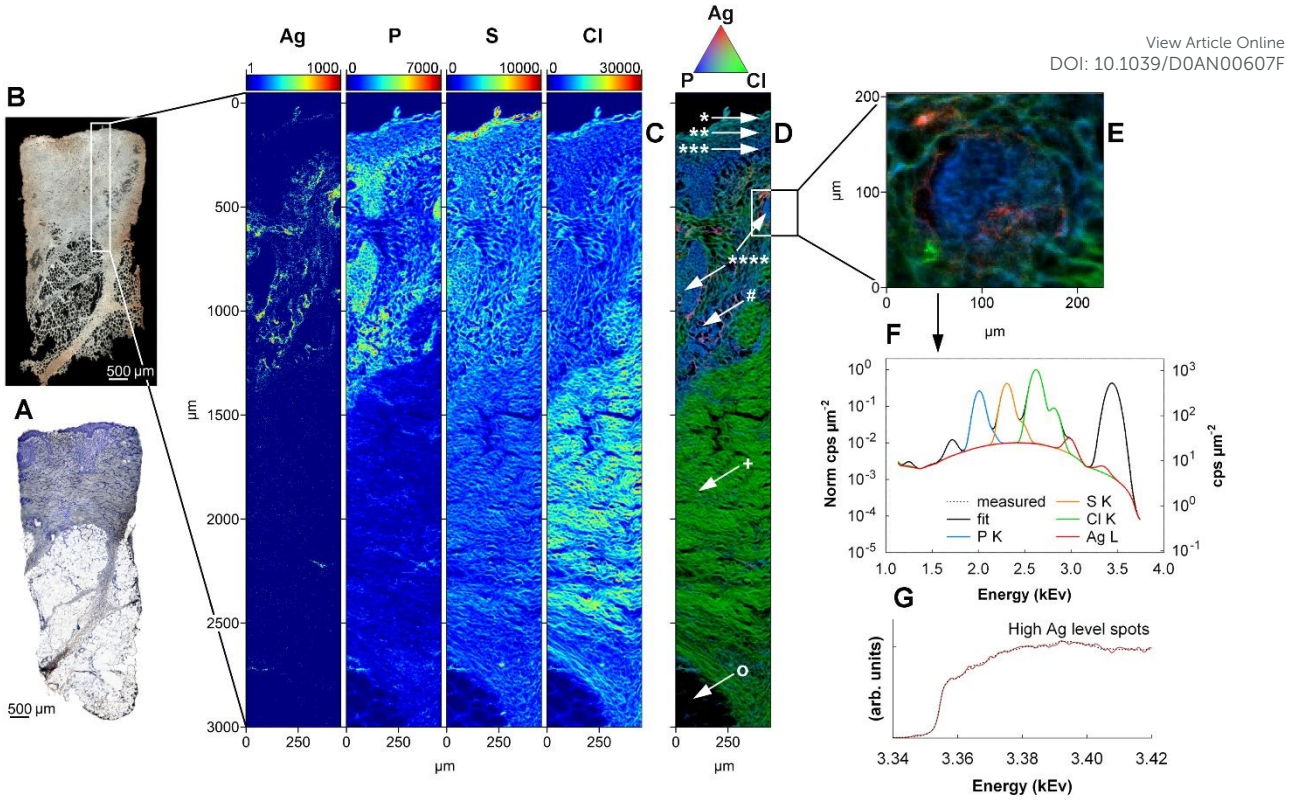

Figure 3. Full profile biopsy specimen of the wound of patient A, 3 days after a single application of the AgNP-containing dressing, analysed by SR-µXRF and SR-XANES. (A) Histological image of the tissue (adjacent slice). (B) Picture of the analysed slice. The scanned area locates in the white frame. (C) Maps of signal intensities (cps) of Ag (log scale), P, S and Cl (linear scales); pixel size 2 µm. (D) Ternary RGB plot of the same elemental maps. The arrows indicate: *stratum corneum; **stratum spinosum; ***stratum basale; ****fragments of epidermis extending in the granulation tissue; #granulation tissue; +reticular dermis; ohypodermis. (E) zoom RGB map of the region located in the frame (independent acquisition, pixel size 2 µm), the arrow indicates the region selected for SR-µXANES analysis; (F) average SR-µXRF spectrum of the whole zoom map area; (G) average SR-µXANES spectrum in the selected region (dotted line) overlapped to its best LCF function (solid line).

View Article Online
DOI: 10.1039/D0AN00607F

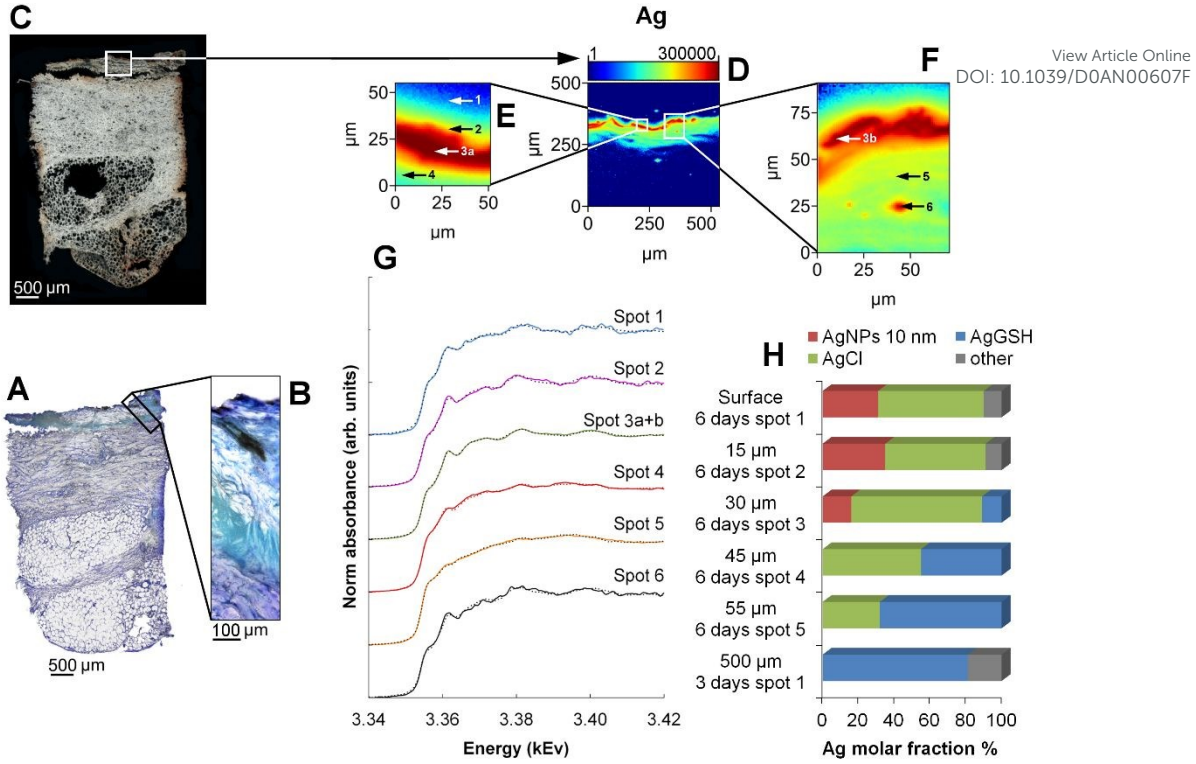

Figure 4. SR-µXRF elemental imaging and spectral data of the skin profile from patient A 6 days after application of the AgNP-containing dressing. (A) histological image of the tissue (adjacent slice) and (B) zoom of the scab region; (C) image of the analysed slice, the upper portion of the scanned area locates in the white frame (for the whole scanned area see Supplementary Fig. S2); (D) map of signal intensity of Ag (cps, logarithmic scale, pixel size 2 µm), the white frames locate the areas selected for independent zoom scans (E) and (F), in which the spots chosen for SR-µXANES analysis are indicated. (G) SR-µXANES spectra of the selected spots (dotted lines) overlapped to their best LCF function (solid lines); (H) Ag speciation as function of the depth along the skin tissue profile, the molar fraction of distinct species was estimated by LCF of the SR-µXANES spectra and are reported in Supplementary Table S1.

View Article Online
DOI: 10.1039/D0AN00607F

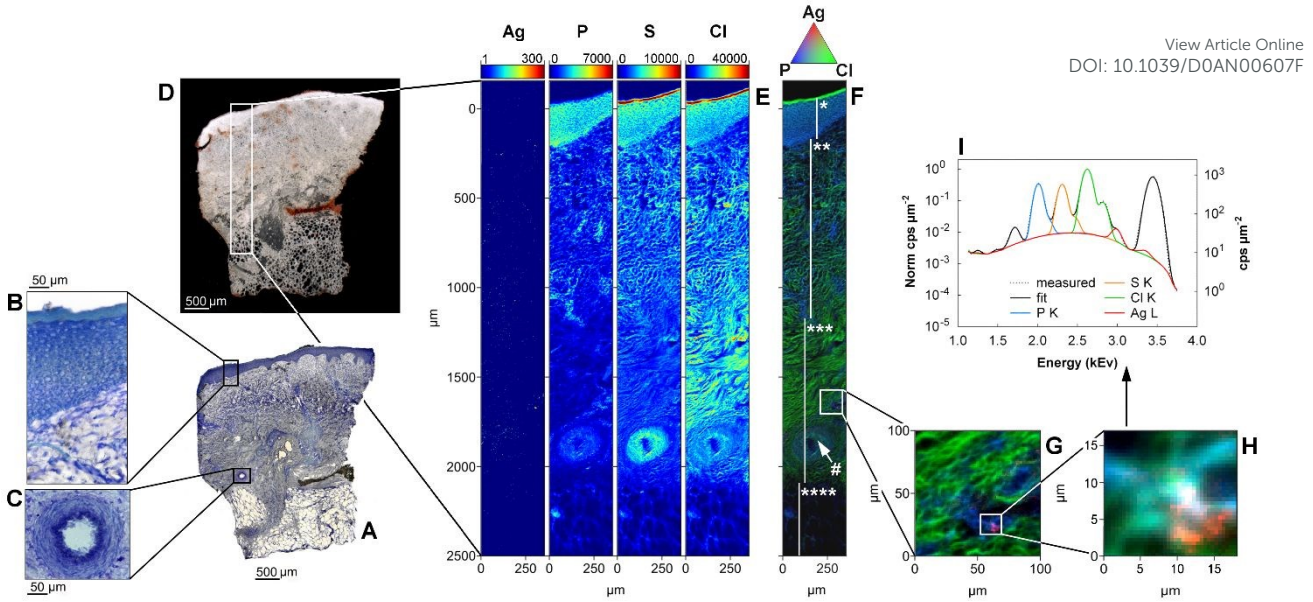

Figure 5. Full profile biopsy specimen of the wound of Patient A, 12 days after a single application of the AgNP-containing dressing (complete healing), analysed by SR-µXRF. (A) Histological image of the tissue (adjacent slice), with zoom images of the regenerated epidermis (B) and an arterial blood vessel (C). (D) Picture of the analysed slice. The scanned area locates in the white frame. (E) Maps of signal intensities (cps) for Ag (logarithmic scale), P, S and Cl (linear scale); pixel size 2 µm. (F) Ternary RGB plot of the same elemental maps. The symbols indicate: *epidermis; **papillary dermis; ***reticular dermis; ****hypodermis; #arterial vessel. (G) and (H): two consecutive zoom maps of the region located in the white frame, independent acquisitions with pixel size 1 µm and 0.5 µm, respectively. (I) Average µXRF spectrum of the whole zoom map area h.

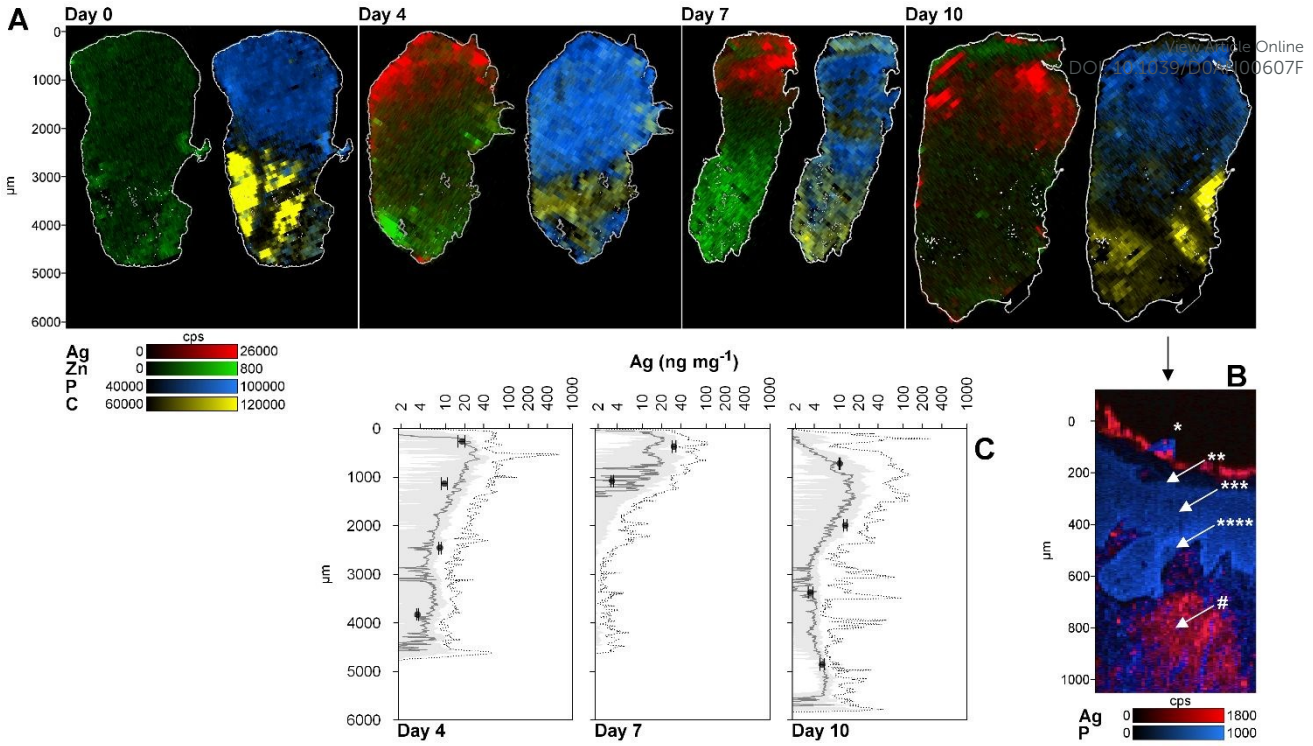

Figure 6. Full profile biopsy specimen of the wound of patient B, before (Day 0) and after repeated applications of the AgNP-containing dressing (Day 4 - 1st app.; Day 7 – 2nd app.; Day 10 = 3rd app., complete healing), analysed by LA-ICP-MS. (A) Maps of signal intensities (cps) for Ag, Zn, P and C (linear scales); pixel size 24 x 100 µm. (B) Detailed map of Ag and P distribution in the surface region of a slice adjacent to the one shown in A)-day 10, pixel size 4 x 12 µm. The arrows indicate: *stratum corneum; **stratum granulosum; ***stratum spinosum; ****stratum basale; #papillary dermis. (C) Depth profiles of Ag concentration in the same samples: the dots are quantitative data (average ± σ) obtained by mineralization and ICP-MS analysis of biopsy residues. Curves are semi-quantitative estimations obtained from the imaging data in a): median (dark line), interquartile range (grey band) and maximum value of the lateral distribution (vertical resolution 14 µm).

View Article Online
DOI: 10.1039/D0AN00607F

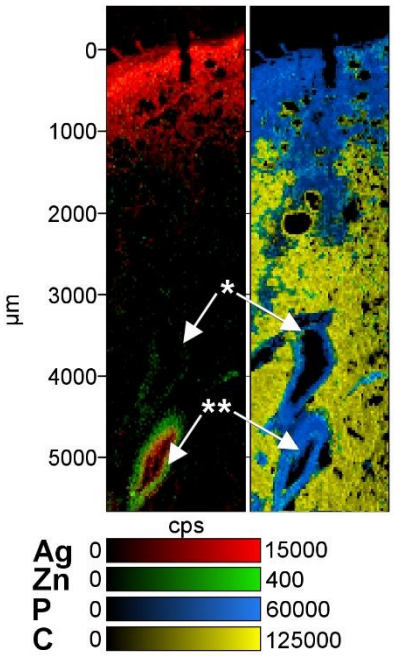

Figure 7. Maps of Ag, Zn, P and C distribution in the skin profile from patient C after 15 days of treatment with repeated applications of the AgNP-containing dressing. Data obtained by LA-ICP-MS with pixel size 24 x 30 µm; signal intensity in cps with linear scale. The arrows indicate: *vein; **artery.

View Article Online
DOI: 10.1039/D0AN00607F

Table of contents entry: highlights

First observation of AgNPs dynamics in the wounds of real patients through elemental imaging and speciation

View Article Online
DOI: 10.1039/D0AN00607F